AIMS Materials Science, 8(5): 698–715.
DOI: 10.3934/matersci.2021042
Received: 07 July 2021
Accepted: 07 September 2021
Published: 17 September 2021

http://www.aimspress.com/journal/Materials

Research article

Optimal weld bead profiles in the conduction mode LBW of thin Ti–6Al–4V alloy sheets

Harish Mooli, Srinivasa Rao Seeram, Satyanarayana Goteti, Nageswara Rao Boggarapu*

Department of Mechanical Engineering, Koneru Lakshmaiah Education Foundation, Deemed to be University, Green Fields, Vaddeswaram, Guntur, 522 502, India

* **Correspondence:** Email: bnrao52@kluniversity.in; Tel: +918106762175.

Abstract: Day by day laser welding (LW) is gaining industrial importance. Good quality of weld joints can be realized through this process. Because this process yields low distortion and small weld bead. Aerospace, nuclear, automotive, and biomedical industries are opting for the lightweight and corrosion resistance titanium alloys. This paper deals with the generation of optimal weld bead profiles in the conduction mode laser beam welding (LBW) of thin Ti–6Al–4V alloy sheets. Laser beam diameter, power and welding speed are the 3 LBW parameters, whereas, bead width, depth of penetration, heat affected zone and maximum temperature are the performance indicators (PIs). 3 levels are set for each LBW parameter. Taguchi's L_9 OA (orthogonal array) is selected to minimize the numerical simulations. ANSYS Fluent V16.0 with Vc++ code is used to develop a generic model. %Contribution of each process variable on the PIs is assessed performing ANOVA analysis. The range of PIs is assessed adopting the modified Taguchi approach. A set of optimal LBW parameters are identified considering a multi-objective optimization technique. For these optimal LBW parameters weld bead width is minimum, and the depth of penetration is maximum. Empirical relations for PIs are developed and validated with simulations. Utilizing the Taguchi's design of experiments, empirical relations are developed for the performance indicators in laser beam welding (LBW) simulations performing few trial runs and identified the optimal LBW process parameters.

Keywords: ANSYS Fluent; power; welding speed; bead width; depth of penetration; laser beam diameter

1. Introduction

Because of small fusion zone and low distortion, laser welding (LW) is gaining industrial importance day by day. Weld quality depends on the weld bead geometry [1–3]. Titanium alloys are treated as good corrosion resistance and lightweight materials. They are of great demand in automotive, aerospace, nuclear and biomedical industries [4]. Researchers are in the continuous process of developing models to simplify the time-consuming simulations. For welding of titanium alloys, laser beam welding (LBW) is opted due to its versatility, high specific heat input, and flexibility. For optimal process conditions, its weld strength is close to that of parent material. However, the potential weldability issues are low elongation, corrosion resistance and inferior fatigue properties [5].

Denney and Metzobower have made an interesting discussion on LBW of titanium [6]. Du et al. have carried out LBW (laser beam welding) simulations and presented fully penetrated weld bead geometry profiles [7]. Benyounis et al. have adopted RSM (response surface methodology) and examined the influence of focal position, speed and laser power on the weld bead geometry of medium steel carbon steel [8]. Liao and Yu have examined the weld bead profiles of thin stainless steel sheets performing pulse laser welding by varying the laser energy and incident angle [9]. Akman et al. have examined the effect of pulse duration and energy on DOP (depth of penetration) by analyzing microstructures and strength properties [10]. ANN (artificial neural network) approach is adopted for investigating the weld geometry [11]. Yamashita et al. and Takemori et al. have performed simulations on LW process [12,13].

Sathiya et al. have followed the Taguchi approach and found the optimal LW parameters for alloy 904L [14]. Shanmugam et al. have utilized ANSYS and performed FEA (finite element analysis) for generating weld bead profiles of AISI 304 varying beam power, incident angle and exposure time [15]. Squillace et al. have examined the influence of LBW parameters on morphology, tensile and fatigue properties [16]. Cherepanov et al. have performed simulations on the thermo-physical processes at LW of alloys possessing refractory nanoparticles [17]. Cao et al. have made investigations on the porosities in the LBW of butt joints [18]. Song et al. have analyzed the residual stress distribution in titanium welds [19]. Akbari et al. have performed simulations on pulsed LW of Ti–6Al–4V alloy and observed 2% to 17% deviation in temperature distribution and melt pool geometry [20]. Gao et al. have examined the influence of LW parameters on porosity formation [21]. Gao et al. have achieved better titanium alloy strength properties with medium OLF (overlapping factor) [22]. The shapes of the molten pool from numerical simulations of Azizpour et al. are comparable with measured data [23]. Akbari et al. have adopted an ANN approach and performed simulations for temperature distribution and melt pool geometry [24]. Zhan et al. have made investigations on invar 36 alloy conducting MIG welding and hybrid laser-MIG welding [25]. Zhan et al. have made consistent assessments with experiments on the microstructure of Ti–6Al–2Zr–1Mo–1V LBW joints [26]. Oliveira et al. have made a survey on the joining of NiTi shape memory alloys [27]. LW of NiTi and Ti6Al4V utilizing niobium interlayer is examined in [28]. High quality of weld joints can be produced through fiber LW of AA6061-T6 [29]. Gursel et al. have observed crack risk in Nd:YAG laser welding [30]. Caiazzo et al. have made investigations on LW of 3 mm thick Ti6Al4V alloy plates and recommended optimal LW parameters to lower the undercut and porosity [31]. Kumar et al. have reported the effect of the scanning speed and beam power on the fiber LW of Ti6Al4V alloy [32]. Kumar et al. have performed simulations and LBW tests on 1 mm

thick Ti–6Al–4V alloy sheets varying welding speed and laser power [33]. Samples annealed at 980 ºC yield tensile strength of 1048 MPa, which is above 4% to that of conventional weld samples. Auwal et al. have discussed the effect of LW parameters weld defects [34]. Kumar et al. have reported optimal parameters, which yielded high tensile strength in pulsed Nd:YAG LW of Monel 400 and Hastelloy C276 sheets [35]. Jiang et al. have carried out simulations and experiments on LW of Ti–6Al–4V alloy varying average power, beam diameter and pulse energy [36]. Kumar and Sinha have made investigations on pulsed Nd:YAG LW of Ti6Al4V alloy varying heat input and presented bead profile, micro-hardness and tensile strength [37].

LBW process will be generally either in conduction or in keyhole mode [38]. Welding in conduction mode is carried out above melting and below vaporization of materials. Thermal convection due to Marangoni flow will be there in addition to heat conduction. In keyhole welding, the surface temperature is above the threshold of boiling point. A hole will be formed in the weld pool after vaporization. Defects (like spatter and blowholes) are introduced upon creation of strong recoil pressure on the melt in the keyhole welding process. Conduction welding is a stable process. It is possible to achieve high quality welds free of pores and spatter [39]. To perform good quality of welding, there is a need for reliable simulation tools and weld equipment's [40,41]. Numerical simulations are required to minimize the cost and time-consuming trial tests, which provide the temperature field and the weld bead geometry. High-speed video recording is required to examine the process on the weld pool surface.

This paper adopts the Taguchi's L_9 OA (orthogonal array) in the numerical simulations to obtain optimal LBW process parameters for thin Ti–6Al–4V alloy sheets. By utilizing the Taguchi's design of experiments, empirical relations are developed for performance indicators in LBW simulations performing few trial runs. Narrow weld bead width with full depth of penetration is arrived by varying the LBW parameters. Empirical relations represent the weld bead profile. A set of optimal LBW parameters is finalized adopting a multi-objective optimization procedure.

2. Materials and methods

Thermal history in the weld is essential for assessing the strength of weld joint. To improve the quality of weld, selection of optimal LBW parameters plays an important role. The time-consuming trial and error-based methods are expensive. A CFD Model is required for carrying out thermo-fluid analysis to generate the weld bead profile. A 3D model for LBW is developed (incorporating buoyancy and Marnangoni stress). ANSYS Fluent embodied with VC++ code is utilized to assess the generic nature of the model by comparing the measured weld bead profiles of different materials (viz., SS304L, carbon steel, zircoly-4 and Zr-1%Nb) [42–47]. In the present study, 2 mm thick Ti–6Al–4V alloy plates (having 50mm length and 20mm width) are considered to perform LBW simulations. Figure 1 shows the LBW parameters and performance indicators. For the 3 LBW process parameters with 3 levels, full factorial design of experiments requires 27 tests, whereas 9 tests are needed as per the Taguchi's L_9 OA.

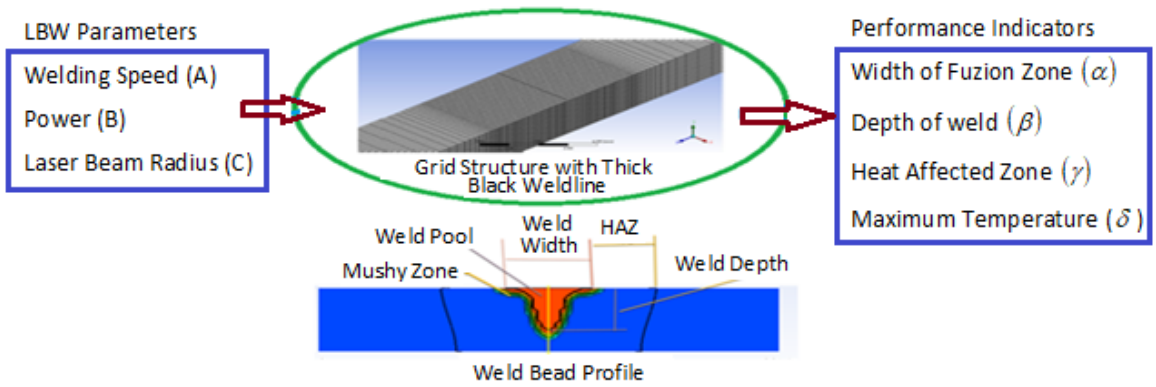

Figure 1. LBW process parameters and the performance indicators.

Numerical simulations are performed by varying 8 to 12 m/s welding speed; 150 to 250 W power; and 0.5 to 1.5 mm laser beam diameter. As in [43], the simulations are based on the solution of N–S (Navier–Stokes) equations, k-ε equation in the regions of mushy zone and weld pool. The temperature dependent properties of Ti–6Al–4V alloy are considered [48]. Specific heat of solid is 670 J/(kg·K), whereas in case liquids it is 730 J/(kg·K). Viscosity of liquid is 0.005 kg/(m·s). Melting heat is 370000 J/kg. Solidus temperature (T_s) is 1878 K. Liquidus temperature (T_L) is 1928 K.

Density, ρ (kg/m^3) in terms of temperature, T (K) is Eq 1.

$$\begin{aligned} \rho &= 4466.2 - 0.154\,T \quad for\ T < 1878\,K \\ &= 31.34\,T - 18467 \quad for\ 1878 < T < 1928\,K \\ &= 5076.8 - 0.68\,T \quad for\ T > 1928\,K \end{aligned} \tag{1}$$

The source term (or momentum frictional dissipation) in the mushy zone is Eq 2 [49,50].

$$\begin{aligned} \vec{S}_w &= 10^3\,\vec{w}\,A_{mush} \quad for\ T < 1878\,K \\ &= \{(0.02T - 37.56)^3 + 10^{-3}\}^{-1} \times (38.56 - 0.02)^2 A_{mush} \quad for\ 1878 < T < 1928\,K \\ &= 0 \quad for\ T > 1928\,K \end{aligned} \tag{2}$$

Here $\vec{w}$ is the pull velocity and A_{mush} is a constant of the mushy zone.

Thermal conductivity, κ ($W{\cdot}m^{-1}{\cdot}K^{-1}$) in terms of T (K) is Eq 3.

$$\begin{aligned} \kappa &= -0.32 + 1.46 \times 10^{-2}\,T \quad for\ 1400 < T < 1850\,K \\ &= -6.66 + 1.83 \times 10^{-2}\,T \quad for\ 1950 < T < 2700\,K \end{aligned} \tag{3}$$

Following the welding process simulations [42–47] and considering the Ti–6Al–4V alloy properties, weld pool cross-section is generated specifying the welding speed (A), power (B) and the laser beam diameter (C) as per Taguchi's L_9 OA. Details on the identification of optimal LBW parameters are presented in the next section.

3. Results

Taguchi method is useful to design with few welding experiments for the process variables and the assigned levels. Analysis of variance (ANOVA) results will be helpful in identifying the optimal

welding parameters. From the experimental data, it is possible to generate the data for the full factorial design of experiments. A simple statistical approach, known as the Taguchi method [51] recommends an orthogonal array (OA) to perform few tests for obtaining performance indicators (PIs). From these tests, it is possible to generate PIs for all combinations of the levels of input process variables. That is the possibility of generating data for the full factorial design of experiments. Obviously, this approach minimizes the cost as well as the time-consuming trial and error-based tests. A few of the successfully solved engineering/industrial optimization problems are damages due to drilling of composites [52–55], stage and satellite separation problems in space vehicles [56–58], performance of heat exchangers [59], design of planetary gears [60,61], welding process [62–67], machining process [68–73], and fuel engine performance [74–77].

Taguchi method [51] recommends L_9 OA for LBW process variables, $n_{pv} = 3$ with levels, $n_{vl} = 3$. The minimum test runs (N_{tests}) required is Eq 4.

$$N_{tests} = 1 + n_{pv} \times (n_{vl} - 1) = 1 + 3 \times (3 - 1) = 7 \quad (4)$$

This could be the reason why Taguchi method [51] recommends L_9 OA. Tables 1 and 2, Figure 2 present numerical simulations of the PIs (viz., width of fusion zone, α (mm), depth of weld, β (mm), heat affected zone, γ (mm) and maximum temperature, δ (K)) and the simulated weld bead profiles for the nine test runs. Substituting $N_{tests} = 9$ and $n_{vl} = 3$ in Eq 4, one gets $n_{pv} = 4$, which indicates the possibility of accommodating 4 process variables in 9 test runs. Modelling and Numerical simulations (utilizing ANSYS Fluent V16.0 with Vc++ code) are validated by comparing the measured weld bead profiles of different materials (viz., SS304L, carbon steel, zircoly-4 and Zr-1%Nb) [42–47]. As in [43], Table 1 introduces a fictitious parameter (D). ANOVA (analysis of variance) results are presented in Table 3. %Contribution of B is significant on the grand mean value of both α and β. %Contribution of A, B and C on α are 8.3%, 88.5% and 2.6% respectively, whereas 26.8%, 52.7% and 19.4% are respectively on β. Sum of the %Contributions of A, B and C on α and β are 99.5% and 99%. Hence, the %Contribution of D on both α and β are 0.5% and 1%, which are nothing but the error (%).

From ANOVA Table 3, the optimal LBW process variables to achieve minimum α (width of fusion zone) are $A_3B_1C_3$, in which subscripts denote the levels of the process variables. The optimal LBW process variables to achieve maximum β (depth of weld) are $A_1B_3C_1$. These two sets of optimal LBW process variables are found to be different for achieving minimum α and maximum β. If the set of LBW process variables is not in L_9 OA of Table 2, then confirmation tests to obtain the PIs are mandatory.

Table 1. Levels of LBW parameters for Ti–6Al–4V alloy.

LBW parameters	Designation	Level-1	Level-2	Level-3
Welding speed (mm/sec)	A	8	10	12
Power (W)	B	150	200	250
Laser beam diameter (mm)	C	0.5	1.0	1.5
Fictitious	D	d_1	d_2	d_3

Table 2. Performance indicators as per Taguchi's L_9 OA.

Test S. No.	LBW parameters (levels)				Performance indicators			
	A	B	C	D	α (mm)	β (mm)	γ (mm)	δ (K)
1	1	1	1	1	2.062	1.597	1.545	2887
2	1	2	2	2	2.796	2.000	1.489	2889
3	1	3	3	3	3.438	2.000	1.491	2591
4	2	1	2	3	1.651	1.090	1.227	2443
5	2	2	3	1	2.218	1.186	1.257	2415
6	2	3	1	2	3.390	2.000	1.454	3617
7	3	1	3	2	1.454	0.696	1.058	2197
8	3	2	1	3	2.458	1.684	1.397	3330
9	3	3	2	1	3.008	1.681	1.344	2895

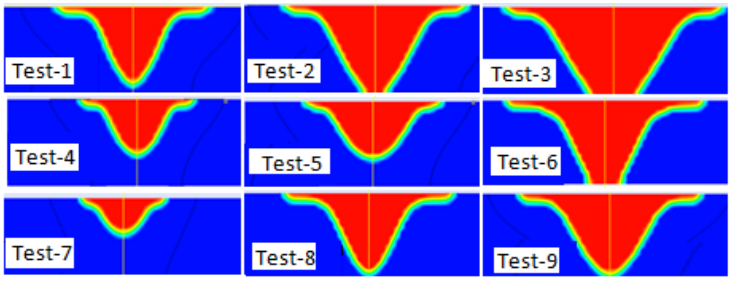

Figure 2. Simulated weld bead profiles for the L_9 OA of test runs.

Table 3. %Contribution of LBW parameters through ANOVA.

	LBW parameters	1 – *Mean*	2 − *Mean*	3 – *Mean*	Sum of squares	%Contribution
Width of fusion zone, α (mm): grand mean = 2.497	A	2.765	2.420	2.307	0.343	8.3
	B	1.722	2.491	3.279	3.633	88.5
	C	2.637	2.485	2.370	0.107	2.6
	D	2.429	2.547	2.516	0.022	0.5
Depth of weld penetration, β (mm): grand mean = 1.548	A	1.886	1.425	1.354	0.461	26.8
	B	1.128	1.623	1.894	0.906	52.7
	C	1.760	1.590	1.294	0.334	19.4
	D	1.488	1.565	1.591	0.017	1.0
Heat affected zone, γ (mm): grand mean = 1.362	A	1.508	1.313	1.266	0.099	50.0
	B	1.277	1.381	1.430	0.037	18.5
	C	1.465	1.353	1.269	0.058	29.5
	D	1.382	1.334	1.372	0.004	2.0
Maximum Temperature, δ (K): grand mean = 2807.1	A	2789	2825	2807	1944	0.1
	B	2509	2878	3034	436576	26.4
	C	3278	2742	2401	1172576	70.8
	D	2732	2901	2788	44316	2.7

Utilizing the additive law [51], estimates of PIs from the results of ANOVA Table 3 obtained are as follows. Let Ψ be the PI and $\widehat{\Psi}$ is its estimate for the process variables (A_i, B_j, C_k, D_l) in which the levels are indicated by subscripts i, j, k, l varying from 1 to 3. Designating $\Psi(A_i)$, $\Psi(B_j)$, $\Psi(C_k)$ and $\Psi(D_l)$ as mean values of Ψ corresponding to the levels of the respective process variables. Ψ_{mean}, is the grand mean of the PI for nine test runs. As per the additive law [51], estimate $\widehat{\Psi}$ for the specified (A_i, B_j, C_k, D_l) is Eq 5.

$$\widehat{\Psi} = \Psi(A_i, B_j, C_k, D_l) = \Psi_{mean} + (\Psi(A_i) - \Psi_{mean}) + (\Psi(B_j) - \Psi_{mean}) + (\Psi(C_k) - \Psi_{mean}) + (\Psi(D_l) - \Psi_{mean}) \quad (5)$$

In case of 3 input variables (A_i, B_j, C_k), Eq 5 reduces to Eq 6.

$$\widehat{\Psi} = \Psi(A_i, B_j, C_k,) = \Psi_{mean} + (\Psi(A_i) - \Psi_{mean}) + (\Psi(B_j) - \Psi_{mean}) + (\Psi(C_k) - \Psi_{mean}) \quad (6)$$

The deviation of the estimates from Eqs 5 and 6 is $\Psi(D_l) - \Psi_{mean}$. For 3 levels (l = 1, 2, 3), 3 deviations are obtained. As in [43], the range of estimates is obtained through superposition of the minimum and maximum deviations to the estimates of Eq 6. Numerical simulations of α, β, γ and δ in Tables 4–7 are within the range of estimates. The minimum and maximum deviations for α, β, γ and δ are (−0.07, 0.05), (−0.06, 0.04), (−0.029, 0.02) and (−74.8, 98.9) respectively.

Table 4. Width of fusion zone, α (mm) from the additive law.

Test S. No.	Simulation	Eq 6 (n_{pv} = 3)	RE (%)	Eq 5 (n_{pv} = 4)	Range of estimates	
					From	To
1	2.062	2.130	−3.3	2.062	2.062	2.179
2	2.796	2.747	1.8	2.796	2.679	2.796
3	3.438	3.420	0.5	3.438	3.352	3.469
4	1.651	1.633	1.1	1.651	1.565	1.682
5	2.218	2.286	−3.1	2.218	2.218	2.335
6	3.390	3.341	1.4	3.390	3.273	3.390
7	1.454	1.405	3.4	1.454	1.337	1.454
8	2.458	2.440	0.7	2.458	2.372	2.489
9	3.008	3.076	−2.3	3.008	3.008	3.125

Table 5. Depth of penetration, β (mm) from additive law.

Test S. No.	Simulation	Eq 6 (n_{pv} = 3)	RE (%)	Eq 5 (n_{pv} = 4)	Range of estimates	
					From	To
1	1.597	1.66	−3.9	1.597	1.597	1.700
2	2.000	1.98	1.0	2.000	1.923	2.026
3	2.000	1.96	2.0	2.000	1.897	2.000
4	1.090	1.05	3.7	1.090	0.987	1.090
5	1.186	1.25	−5.4	1.186	1.186	1.289
6	2.000	1.98	1.0	2.000	1.923	2.026
7	0.696	0.68	2.3	0.696	0.619	0.722
8	1.684	1.64	2.6	1.684	1.581	1.684
9	1.681	1.74	−3.5	1.681	1.681	1.784

Table 6. Heat affected zone, γ (mm) from the additive law.

Test S. No.	Simulation	Eq 6 (n_{pv} = 3)	RE (%)	Eq 5 (n_{pv} = 4)	Range of estimates	
					From	To
1	1.545	1.525	1.3	1.545	1.497	1.545
2	1.489	1.518	−1.9	1.489	1.489	1.537
3	1.491	1.482	0.6	1.491	1.453	1.501
4	1.227	1.218	0.7	1.227	1.189	1.237
5	1.257	1.237	1.6	1.257	1.209	1.257
6	1.454	1.483	−2.0	1.454	1.454	1.502
7	1.058	1.087	−2.7	1.058	1.058	1.106
8	1.397	1.388	0.6	1.397	1.359	1.407
9	1.344	1.324	1.5	1.344	1.296	1.344

Table 7. Maximum temperature, δ (K) from the additive law.

Test S. No.	Simulation	Eq 6 (n_{pv} = 3)	RE (%)	Eq 5 (n_{pv} = 4)	Range of estimates	
					From	To
1	2887	2961	−2.6	2887	2887	3055
2	2889	2795	3.2	2889	2720	2889
3	2591	2610	−0.7	2591	2535	2704
4	2443	2462	−0.8	2443	2387	2556
5	2415	2490	−3.1	2415	2415	2583
6	3617	3523	2.6	3617	3448	3617
7	2197	2103	4.3	2197	2028	2197
8	3330	3349	−0.6	3330	3274	3443
9	2895	2970	−2.6	2895	2895	3063

Following the concept of additive law, empirical relations for the PIs (α, β, γ and δ) are developed (from the results of ANOVA Table 3) in the form Eqs 7–10.

$$\alpha = 2.401 - 0.229\xi_1 + 0.116\xi_1^2 + 0.778\xi_2 + 0.01\xi_2^2 - 0.133\xi_3 + 0.018\xi_3^2 \quad (7)$$

$$\beta = 1.543 - 0.256\xi_1 + 0.184\xi_1^2 + 0.383\xi_2 - 0.113\xi_2^2 - 0.233\xi_3 - 0.063\xi_3^2 \quad (8)$$

$$\gamma = 1.322 - 0.121\xi_1 + 0.075\xi_1^2 + 0.077\xi_2 - 0.028\xi_2^2 - 0.098\xi_3 + 0.014\xi_3^2 \quad (9)$$

$$\delta = 2831 + 9.17\xi_1 - 26.83\xi_1^2 + 262.67\xi_2 - 106.33\xi_2^2 - 438.5\xi_3 + 97.17\xi_3^2 \quad (10)$$

Here $\zeta_1 = 0.5A - 5$; $\zeta_2 = 0.02B - 4$; and $\zeta_3 = 2C - 2$. The range of estimates for PIs (α, β, γ and δ) from empirical relations Eqs 7–10 is obtained by superimposing the respective minimum and maximum deviations. Figures 3–6 show the estimates of α, β, γ and δ for all possible 27 combinations ((($A_iB_jC_k$), k = 1, 2, 3), j = 1, 2, 3), i = 1, 2, 3) of LBW parameters. Numerical simulations in Table 2 for the test runs in these Figures 3–6 are within the expected range (that is within lower and upper bounds).

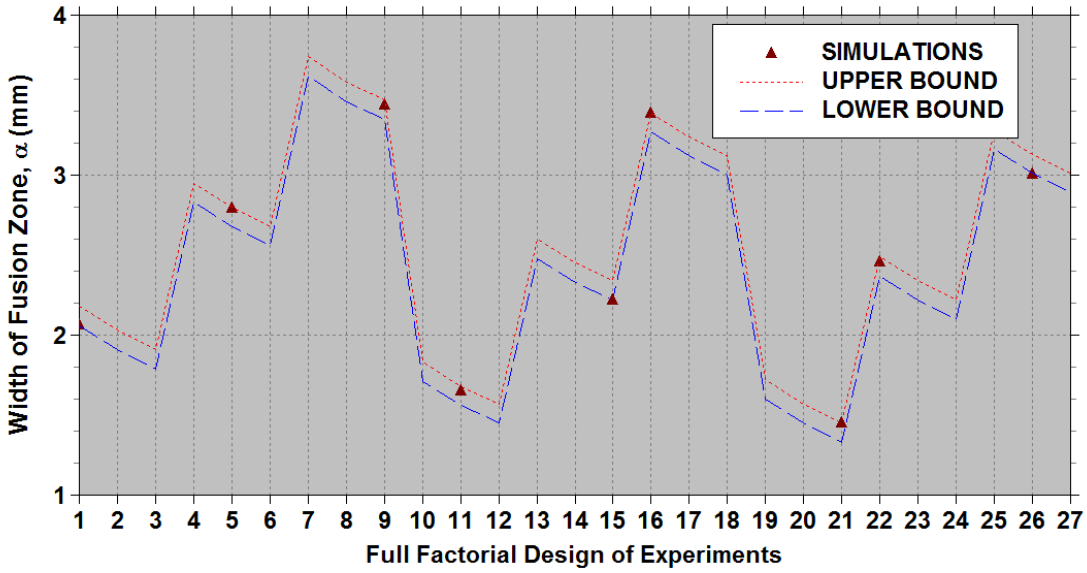

Figure 3. Width of fusion zone from the empirical relation Eq 7.

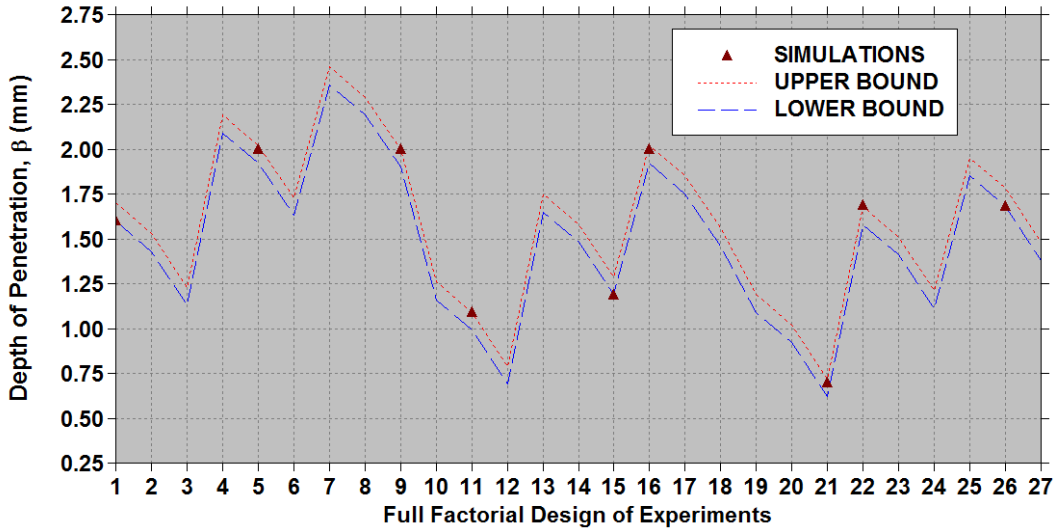

Figure 4. Depth of penetration from the empirical relation Eq 8.

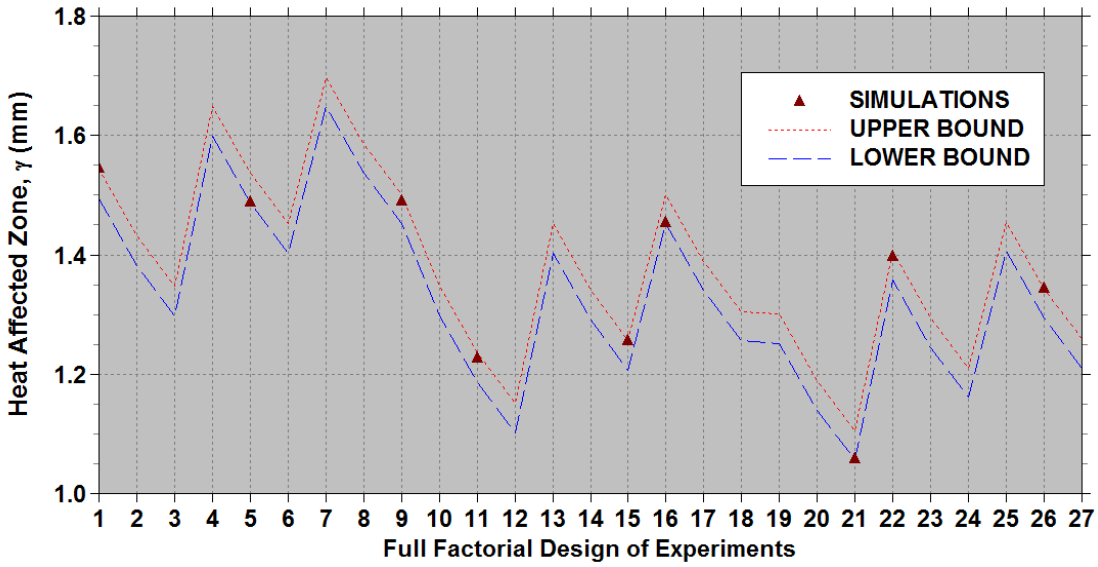

Figure 5. Heat affected zone from the empirical relation Eq 9.

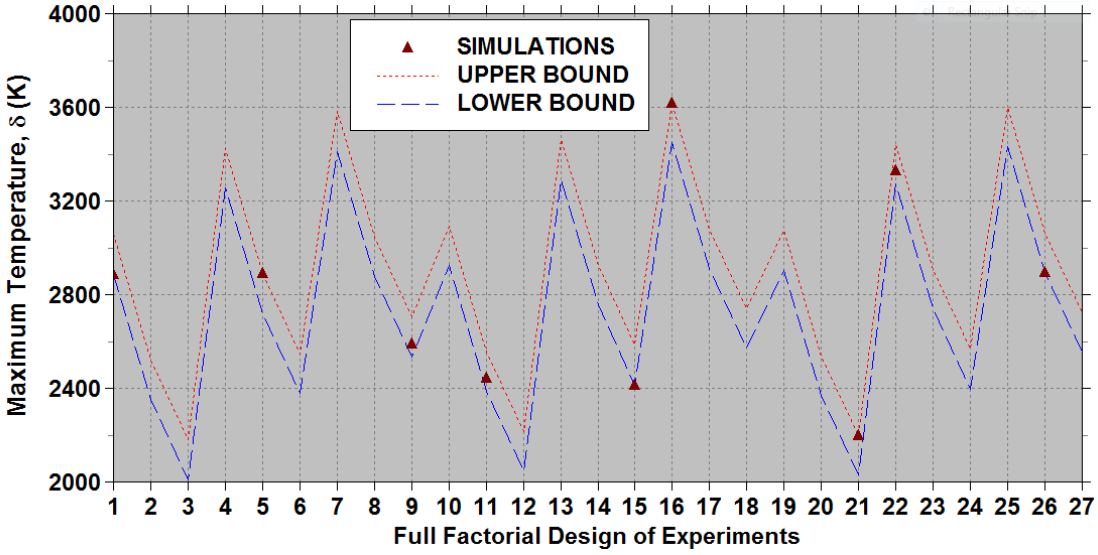

Figure 6. Maximum temperature from empirical relation Eq 10.

4. Results and discussion

($A_3B_1C_3$) and ($A_1B_3C_1$) are two different sets of input process variables identified for minimum α and maximum β. To select a set of input process variables, a multi-objective optimization technique [64,65] is followed here by constructing a single objective function (ζ) in terms of α and β (after normalizing with α_{max} and β_{max}) and introducing weighing factors $\omega_1 \in [0, 1]$ and $\omega_2 = 1 - \omega_1$.

The single objective function (ζ) is Eq 11.

$$\zeta = \omega_1 \zeta_1 + \omega_2 \zeta_2 = \omega_1 \left(\frac{\alpha}{\alpha_{\max}}\right) + \omega_2 \left(\frac{\beta_{\max}}{\beta} - 1\right) \tag{11}$$

Minimization of ζ implies maximization of β and minimization of α for a set of input process variables. Table 8 presents the data for ζ generated from Table 8 consider equal weighting ($\omega_1 = \omega_2 = \frac{1}{2}$). ANOVA results are also presented in Table 8. The optimal input variables selected for the minimum ζ are $A_1B_2C_1$. These correspond to welding speed = 8 mm/s; power = 200 W and laser beam diameter = 0.5 mm. The PIs for these input variables are not in the Taguchi L_9 OA of Table 1. Hence, numerical simulations are performed by specifying the identified optimal input variables for obtaining the weld bead profile. Table 9 gives weld bead profiles for the single and multiple objective optimization problems. Numerical simulations are comparable to the range of PIs estimated from empirical relations Eqs 7–10. Figures 7–9 show the weld bead profile for max depth of weld, minimum bead width and optimum depth and width.

Table 8. ANOVA results on the optimization function (ζ) for the simulated PIs in Table 1. (α_{max} = 3.438 mm, β_{max} = 2.00 mm, $\omega_1 = \omega_2 = 1/2$).

Test S. No.	LBW parameters			$\zeta_1\left(=\frac{\alpha}{\alpha_{max}}\right)$	$\zeta_2\left(\frac{\beta_{max}}{\beta}-1\right)$	$\zeta\ (=\omega_1\zeta_1+\omega_2\zeta_2)$ Eq 11
	A (mm/s)	B (W)	C (mm)			
1	8	150	0.5	0.600	0.252	0.426
2	8	200	1.0	0.813	0	0.407
3	8	250	1.5	1.000	0	0.500
4	10	150	1.0	0.480	0.835	0.658
5	10	200	1.5	0.645	0.686	0.666
6	10	250	0.5	0.986	0.000	0.493
7	12	150	1.5	0.423	1.874	1.148
8	12	200	0.5	0.715	0.188	0.451
9	12	250	1.0	0.875	0.190	0.532
ANOVA results on ζ						
1 − Mean	0.4443	0.7440	0.4567	-	-	-
2 − Mean	0.6057	0.5080	0.5323	-	-	-
3 − Mean	0.7103	0.5083	0.7713	-	-	-

Table 9. Simulation results with estimates for the specific optimal LBW parameters.

Optimum LBW parameters	Approach	Width of fusion zone, α (mm)	Depth of weld, β (mm)	Size of HAZ, γ (mm)	Maximum temperature, δ (mm)
Maximum depth of weld: $A_1B_3C_1$ (ω_1 = 0, ω_2 = 1)	Simulations	4.02	2	1.602	3445
	Additive law	3.686	2.42	1.678	3487
	Expected range	3.618–3.736	2.363–2.466	1.650–1.698	3412–3581
Minimum width: $A_3B_1C_3$ (ω_1 = 1, ω_2 = 0)	Simulations	1.454	0.696	1.058	2197
	Additive law	1.405	0.680	1.087	2103
	Expected range	1.337–1.454	0.619–0.722	1.058–1.106	2028–2197
Optimum depth and width: $A_1B_2C_1$ (ω_1 = ω_2 = 0.5)	Simulations	3.048	2	1.576	3194
	Additive law	2.898	2.15	1.630	3330
	Expected range	2.830–2.948	2.093–2.196	1.601–1.649	3256–3424

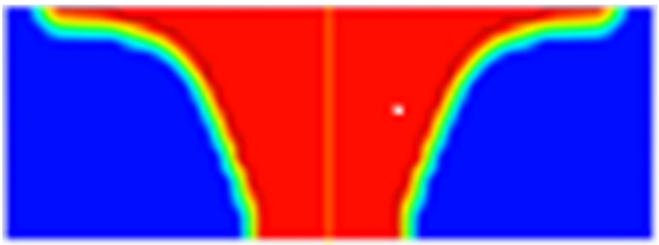

Figure 7. Wed bead profile for maximum depth of weld (ω_1 = 0, ω_2 = 1).

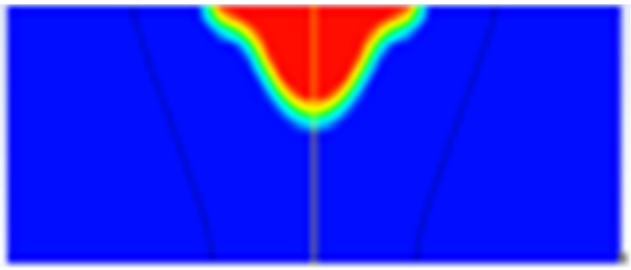

Figure 8. Wed bead profile for minimum bead width ($\omega_1 = 1$, $\omega_2 = 0$).

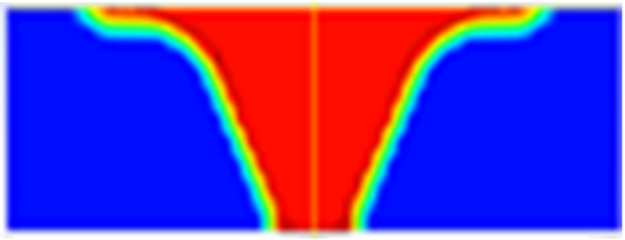

Figure 9. Wed bead profile for optimum depth and width ($\omega_1 = \omega_2 = 0.5$).

5. Conclusions

Numerical simulations are performed on the laser beam welding (LBW) of 2 mm thick Ti–6Al–4V alloy sheets. Taguchi's design of experiments is followed to conduct few simulations. Following the concept of additive law in Taguchi's approach, the performance indicators (PIs), namely, width of fusion zone (α) and depth of penetration (β) are estimated and validated with simulation results for the input process variables in each test run of the Taguchi's L_9 OA (orthogonal array).

- Empirical relations are developed for PIs.
- Modified Taguchi approach provides the range of estimates for PIs.
- Optimal LBW process parameters are identified through a multi-objective optimization.
- Numerical simulations for the optimal LBW parameters are within the range of estimates.
- Incorporation of Taguchi approach in numerical simulations minimizes the trial and error-based test runs thereby reduction in computational time in selecting the optimal LBW parameters.

Future work is directed towards experimentation for investigating the microstructures and formation of defects in welding of Ti–6Al–4V with different welding processes (viz., electron beam welding, laser beam welding, plasma arc welding and TIG welding), and their influence on the properties.

Acknowledgments

The authors wish to thank the authorities of Koneru Lakshmaiah Education Foundation, India for providing facilities to carry out this work. The authors are grateful to the reviewers for their constructive criticism to improve the quality of presentation.

Conflict of interest

All authors declare no conflicts of interest in this paper.

References

1. Oliveira JP, Schell N, Zhou N, et al. (2019) Laser welding of precipitation strengthened Ni-rich NiTiHf high temperature shape memory alloys: Microstructure and mechanical properties. *Mater Design* 162: 229–234.
2. Oliveira JP, Shen J, Escobar JD, et al. (2021) Laser welding of H-phase strengthened Ni-rich NiTi-20Zr high temperature shape memory alloy. *Mater Design* 202: 109533.
3. Shamsolhodaei A, Oliveira JP, Schell N, et al. (2020) Controlling intermetallic compounds formation during laser welding of NiTi to 316L stainless steel. *Intermetallics* 116: 106656.
4. Wang SH, Wei MD, Tsay LW (2003) Tensile properties of LBW welds in Ti–6Al–4V alloy at evaluated temperatures below 450 ºC. *Mater Lett* 57: 1815–1823.
5. Auwal ST, Ramesh S, Yusof F, et al. (2018) A review on laser beam welding of titanium alloys. *Int J Adv Manuf Technol* 97: 1071–1098.
6. Denney PE, Metzbower EA (1989) Laser beam welding of titanium. *Weld J* 68: 342–346.
7. Du H, Hu L, Liu J, et al. (2004) A study on the metal flow in full penetration laser beam welding for titanium alloy. *Comp Mater Sci* 29: 419–427.
8. Benyounis KY, Olabi AG, Hashmi MSJ (2005) Effect of laser welding parameters on the heat input and weld-bead profile. *J Mater Process Tech* 164: 978–985.
9. Liao YC, Yu MH (2007) Effects of laser beam energy and incident angle on the pulse laser welding of stainless steel thin sheet. *J Mater Process Tech* 190: 102–108.
10. Akman E, Demir A, Canel T, et al. (2009) Laser welding of Ti6Al4V titanium alloys. *J Mater Process Tech* 209: 3705–3713.
11. Khorram A, Yazdi MRS, Ghoreishi M, et al. (2010) Using ANN approach to investigate the weld geometry of Ti 6Al 4V Titanium Alloy. *Int J Eng Technol* 2: 491.
12. Yamashita S, Yonemoto Y, Yamada T, et al. (2010) Numerical simulation of laser welding processes with CIP finite volume method. *Trans JWRI* 39: 37–39.
13. Takemori CK, Muller DT, Oliveira MA (2010) Numerical simulation of transient heat transfer during welding process. *International Compressor Engineering Conference at Purdue*, 1–8.
14. Sathiya P, Jaleel MYA, Katherasan D, et al. (2011) Optimization of laser butt welding parameters with multiple performance characteristics. *Opt Laser Technol* 43: 660–673.
15. Shanmugam NS, Buvanashekaran G, Sankaranarayanasamy K (2012) Some studies on weld bead geometries for laser spot welding process using finite element analysis. *Mater Design* 34: 412–426.
16. Squillace A, Prisco U, Ciliberto S, et al. (2012) Effect of welding parameters on morphology and mechanical properties of Ti–6Al–4V laser beam welded butt joints. *J Mater Process Tech* 212: 427–436.
17. Cherepanov AN, Shapeev VP, Liu G, et al. (2012) Simulation of thermophysical processes at laser welding of alloys containing refractory nanoparticles. *AMPC* 2: 270–273.
18. Cao X, Kabir ASH, Wanjara P, et al. (2014) Global and local mechanical properties of autogenously laser welded Ti–6Al–4V. *Metall Mater Trans A* 45: 1258–1272.

19. Song SP, Paradowska AM, Dong PS (2014) Investigation of residual stresses distribution in titanium weldments, *Materials Science Forum*, 777: 171–175.
20. Akbari M, Saedodin S, Toghraie D, et al. (2014) Experimental and numerical investigation of temperature distribution and melt pool geometry during pulsed laser welding of Ti6Al4V alloy. *Opt Laser Technol* 59: 52–59.
21. Gao XL, Zhang LJ, Liu J, et al. (2014) Porosity and microstructure in pulsed Nd:YAG laser welded Ti6Al4V sheet. *J Mater Process Tech* 214: 1316–1325.
22. Gao XL, Liu J, Zhang LJ, et al. (2014) Effect of the overlapping factor on the microstructure and mechanical properties of pulsed Nd:YAG laser welded Ti6Al4V sheets. *Mater Charact* 93: 136–149.
23. Azizpour M, Ghoreishi M, Khorram A (2015) Numerical simulation of laser beam welding of Ti6Al4V sheet. *JCARME* 4: 145–154.
24. Akbari M, Saedodin S, Panjehpour A, et al. Numerical simulation and designing artificial neural network for estimating melt pool geometry and temperature distribution in laser welding of Ti6Al4V alloy. *Optik* 127: 11161–11172.
25. Zhan X, Li Y, Ou W, et al. (2016) Comparison between hybrid laser-MIG welding and MIG welding for the invar36 alloy. *Opt Laser Technol* 85: 75–84.
26. Zhan X, Peng Q, Wei Y, et al. (2017) Experimental and simulation study on the microstructure of TA15 titanium alloy laser beam welded joints. *Opt Laser Technol* 94: 279–289.
27. Oliveira JP, Miranda RM, Fernandes FMB (2017) Welding and joining of NiTi shape memory alloys: a review. *Prog Mater Sci* 88: 412–466.
28. Oliveira JP, Panton B, Zeng Z, et al. (2016) Laser joining of NiTi to Ti6Al4V using a Niobium interlayer. *Acta Mater* 105: 9–15.
29. Su C, Zhou JZ, Ye YX, et al. (2017) Study on fiber laser welding of AA6061-T6 samples through numerical simulation and experiments. *Procedia Eng* 174: 732–739.
30. Gursel A (2017) Crack risk in Nd: YAG laser welding of Ti–6Al–4V alloy. *Mater Lett* 197: 233–235.
31. Caiazzo F, Alfieri V, Astarita A, et al. (2016) Investigation on laser welding of Ti–6Al–4V plates in corner joint. *Adv Mech Eng* 9: 1–9.
32. Kumar C, Das M, Paul CP, et al. (2017) Experimental investigation and metallographic characterization of fiber laser beam welding of Ti–6Al–4V alloy using response surface method. *Opt Laser Eng* 95: 52–68.
33. Kumar U, Gope DK, Srivastava JP, et al. (2018) Experimental and numerical assessment of temperature field and analysis of microstructure and mechanical properties of low power laser annealed welded joints. *Materials* 11: 1514.
34. Auwal ST, Ramesh S, Yusof F, et al. (2018) A review on laser beam welding of titanium alloys. *Int J Adv Manuf Technol* 97: 1071–1098.
35. Kumar GS, Raghukandan K, Saravanan S, et al. (2019) Optimization of parameters to attain higher tensile strength in pulsed Nd:YAG laser welded Hastelloy C-276–Monel 400 sheets. *Infrared Phys Techn* 100: 1–10.
36. Jiang D, Alsagri AS, Akbari M, et al. (2019) Numerical and experimental studies on the effect of varied beam diameter, average power and pulse energy in Nd:YAG laser welding of Ti6Al4V. *Infrared Phys Techn* 101: 180–188.

37. Kumar P, Sinha AN (2019) Effect of heat input in pulsed Nd:YAG laser welding of titanium alloy (Ti6Al4V) on microstructure and mechanical properties. *Weld World* 63: 673–689.
38. Steen WM, Mazumder J (2010) *Laser Material Processing*, 4 Eds., Berlin: Springer Science & Business Media.
39. Assuncao DE, Ganguly S, Yapp D, et al. (2010) Conduction mode: broadening the range of applications for laser welding. *63rd Annual Assembly & International Conference of the International Institute of Welding*, Istanbul, Turkey, 705–709.
40. Shao J, Yan Y (2005) Review of techniques for on-line monitoring and inspection of laser welding, *Journal of Physics: Conference Series*, 15: 017.
41. He X (2012) Finite element analysis of laser welding: a state of art review. *Mater Manuf Process* 27: 1354–1365.
42. Satyanarayana G, Narayana KL, Boggarapu NR (2018) Numerical simulations on the laser spot welding of zirconium alloy endplate for nuclear fuel bundle assembly. *Lasers Manuf Mater Process* 5: 53–70.
43. Satyanarayana G, Narayana KL, Rao BN (2018) Identification of optimum laser beam welding process parameters for E110 zirconium alloy butt joint based on Taguchi-CFD simulations. *Lasers Manuf Mater Process* 5: 182–199.
44. Satyanarayana G, Narayana KL, Rao BN, et al. (2019) Numerical simulation of the processes of formation of a welded joint with a pulsed Nd: YAG laser welding of ZR–1% NB alloy. *Therm Eng* 66: 210–218.
45. Satyanarayana G, Narayana KL, Rao BN (2019) Numerical investigation of temperature distribution and melt pool geometry in laser beam welding of a Zr–1% Nb alloy nuclear fuel rod end cap. *B Mater Sci* 42: 1–9.
46. Satyanarayana G (2019) Thermal and fluid flow simulations in conduction mode laser beam welding of zirconium alloys [PhD's thesis]. K L University: India.
47. Satyanarayana G, Narayana KL, Rao BN (2021) Incorporation of Taguchi approach with CFD simulations on laser welding of spacer grid fuel rod assembly. *Mat Sci Eng B-Solid* 269: 115182.
48. Rai R (2008) Modeling of heat transfer and fluid flow in keyhole mode welding [PhD's thesis]. The Pennsylvania State University: USA.
49. ANSYS (2016) ANSYS Fluent User's Guide. Available form: http://www.pmt.usp.br/academic/martoran/notasmodelosgrad/ANSYS%20Fluent%20Users%20Guide.pdf.
50. Voller VR, Prakash C (1987) A fixed grid numerical modelling methodology for convection-diffusion mushy region phase-change problems. *Int J Heat Mass Tran* 30: 1709–1719.
51. Ross PJ (1996) *Taguchi Techniques for Quality Engineering: Loss Function, Orthogonal Experiments, Parameter and Tolerance Design*, 2 Eds., New York: McGraw-Hill.
52. Rao BS, Rudramoorthy R, Srinivas S, et al. (2008) Effect of drilling induced damage on notched tensile and pin bearing strengths of woven GFR-epoxy composites. *Mat Sci Eng A-Struct* 472: 347–352.
53. Parameshwaranpillai T, Lakshminarayanan PR, Rao BN (2011) Taguchi's approach to examine the effect of drilling induced damage on the notched tensile strength of woven GFR–epoxy composites. *Adv Compos Mater* 20: 261–275.

54. Kumar DR, Varma P, Rao BN (2017) Optimum drilling parameters of coir fiber-reinforced polyester composites. *AJMIE* 2: 92–97.
55. Konduri SSS, Kalavala VMK, Mandala P, et al. (2017) Application of Taguchi approach to seek optimum drilling parameters for woven fabric carbon fibre/epoxy laminates. *MAYFEB J Mech Eng* 1: 29–37.
56. Singaravelu J, Jeyakumar D, Rao BN (2009) Taguchi's approach for reliability and safety assessments in the stage separation process of a multistage launch vehicle. *Reliab Eng Syst Safe* 94: 1526–1541.
57. Singaravelu J, Jeyakumar D, Rao BN (2012) Reliability and safety assessments of the satellite separation process of a typical launch vehicle. *J Def Model Simul* 9: 369–382.
58. Singaravelu J (2011) Reliability and safety assessment on aerospace structural elements and separation systems [PhD's thesis]. University of Kerala: India.
59. Dutta OY, Rao BN (2018) Investigations on the performance of chevron type plate heat exchangers. *Heat Mass Transfer* 54: 227–239.
60. Miladinović S, Veličković S, Karthik K, et al. (2020) Optimal safe factor for surface durability of first central and satellite gear pair in ravigneaux planetary gear set. *Test Eng Manag* 83: 16504–16510.
61. Miladinović S, Veličković S, Loknath D, et al. (2020) Parameters identification and minimization of safety coefficient for surface durability of internal planetary gear using the modified Taguchi approach. *Test Eng Manag* 83: 25108–25116.
62. Sahiti M, Reddy MR, Joshi B, et al. (2016) Optimum WEDM process parameters of Incoloy® Alloy800 using Taguchi method. *Int J Ind Syst Eng* 1: 64–68.
63. Bharathi P, Priyanka TGL, Rao GS, et al. (2016) Optimum WEDM process parameters of SS304 using Taguchi method. *Int J Ind Syst Eng* 1: 69–72.
64. Dharmendra BV, Kodali SP, Rao BN (2019) A simple and reliable Taguchi approach for multi-objective optimization to identify optimal process parameters in nano-powder-mixed electrical discharge machining of INCONEL800 with copper electrode. *Heliyon* 5: e02326.
65. Dharmendra BV, Kodali SP, Boggarapu NR (2020) Multi-objective optimization for optimum abrasive water jet machining process parameters of Inconel718 adopting the Taguchi approach. *Multidiscip Model Mater Struct* 16: 306–321.
66. Harish M, Rao SS, Rao BN (2020) On machining of Ti–6Al–4V alloy and its parameters optimization using the modified Taguchi approach. *Test Eng Manag* 83: 17007–17017.
67. Harish M, Rao SS, Rao BN, et al. (2020) Specific optimal AWJM process parameters for Ti–6Al–4V alloy employing the modified Taguchi approach. *J Math Comput Sci* 11: 292–311.
68. Sahiti M, Reddy MR, Joshi B, et al. (2016) Application of Taguchi method for optimum weld process parameters of pure aluminum. *AJMIE* 1: 123–128.
69. Rajyalakshmi K, Boggarapu NR (2019) Expected range of the output response for the optimum input parameters utilizing the modified Taguchi approach. *Multidiscip Model Mater Struct* 15: 508–522.
70. Rajyalakshmi K, Rao BN (2019) Modified Taguchi approach to trace the optimum GMAW process parameters on weld dilution for ST-37 steel plates. *J Test Eval* 47: 3209–3223.
71. Satyanarayana G, Narayana KL, Rao BN (2019) Optimal laser welding process parameters and expected weld bead profile for P92 steel. *SN Appl Sci* 1: 1–11.

72. Harish M, Prasad VS, Reddy MBSS, et al. (2019) Optimal process parameters to achieve maximum tensile load bearing capacity of laser weld thin galvanized steel sheets. *IJRTE* 8: 11682–11687.
73. Prasad VS, Harish M, Reddy MBSS, et al. (2019) Optimal FSW process parameters to improve the strength of dissimilar AA6061-T6 to Cu welds with Zn interlayer. *IJRTE* 8: 11688–11695.
74. Dey S, Deb M, Das PK (2019) Application of fuzzy-assisted grey Taguchi approach for engine parameters optimization on performance-emission of a CI engine. *Energy Sources Part A* 2019: 1–17.
75. Gul M, Shah AN, Aziz U, et al. (2019) Grey-Taguchi and ANN based optimization of a better performing low-emission diesel engine fueled with biodiesel. *Energy Sources Part A* 2019: 1–14.
76. Venkatanarayana B, Ratnam C (2019) Selection of optimal performance parameters of DI diesel engine using Taguchi approach. *Biofuels* 10: 503–510.
77. Ganesan S, Senthil Kumar J, Hemanandh J (2020) Optimisation of CI engine parameter using blends of biodiesel by the Taguchi method. *Int J Ambient Energy* 41: 205–208.

AIMS Press

©2021 the Author(s), licensee AIMS Press. This is an open access article distributed under the terms of the Creative Commons Attribution License (http://creativecommons.org/licenses/by/4.0)